M. Meyling*, S. Latus, L. Maack, L. Miščikas, M. Rojas, T. Maurer, and A. Schlaefer

Learning-based Target Localization in Robotic Radioguided Surgery in Noisy Environments

https://doi.org/10.1515/cdbme-2025-0323

Abstract: In radioguided surgery, ɣ-probes are used intraoperatively to localize targets marked by radionuclides. However, the interpretation of ɣ-probe measurements is challenging due to background activity from surrounding organs. This work investigated whether deep neural networks can localize radiation sources in such environments and how different background activities impact this task. A physics-guided forward model simulated ɣ-probe measurements for different intra-abdominal distributions, including an anatomically inspired bladder activity. A convolutional neural network was trained on simulated measurements to predict 3D target source positions. Results indicated that prediction accuracy improved with more ɣ-probe measurements and degraded with increased background activity. In particular, proximity to high-activity regions like the bladder significantly reduced accuracy. This study demonstrates the need to consider background activity distributions for target localization and that a convolutional neural network could solve this task.

Keywords: Source Localization, Radio Guided Surgery, Robotic Laparoscopic Surgery

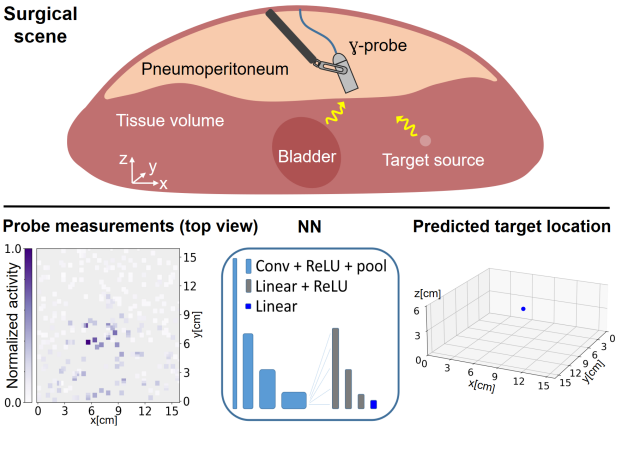

Fig. 1: Top: Surgical setup visualized in a transverse pelvic cross section, z-axis is pointing to the anterior. A ɣ-probe is maneuvered within the pneumoperitoneum to measure radioactivity from both the target source and surrounding tissues. **Bottom:** Measurements acquired for multiple ɣ-probe poses were input to a neural network, which estimated the 3D location of the target source.

1 Introduction

Prostate cancer is the most prevalent cancer among men and can significantly reduce quality of life. Treatment options range from radical prostatectomy to external radiotherapy [1]. To identify disease recurrence and to enable early targeted therapy, radionuclides directed against the prostate-specific membrane antigen (PSMA), a marker for prostate cancer cells, are injected systemically. Then, positron emission tomography combined with computed tomography (PET/CT) is performed. The there identified metastases, e.g. located in lymph nodes, can then be removed surgically.

Surgical approaches have evolved from open procedures to minimally invasive laparoscopic techniques, and more recently, to robotic-assisted laparoscopic surgeries [2]. However, transferring the small target locations from PET/CT imaging to the intraoperative field remains a major challenge. To support intraoperative localization, 99m-Tc-labelled radiotracers against PSMA can be injected prior to surgery, and a ɣ-probe is used to detect the emitted radiation [3]. However, interpreting the ɣ-probe's cues is not intuitive and heavily relies on the surgeon's experience [4]. Additionally, high background activity from radionuclide accumulation in organs such as the bladder contributes significant noise to the measurements [5].

To enhance intraoperative radioguidance, several methods have been proposed, most of which leveraged information about the pose of the ɣ-probe. This pose can be obtained through stereoscopic tracking or derived from the robot's kinematic data. Based on this information, different strategies have been explored: reconstruction of the radionuclide distribution using maximum likelihood expectation maximization [6], es-

***Corresponding author: M. Meyling,** Institute of Medical Technology and Intelligent Systems, Hamburg University of Technology, Am Schwarzenberg-Campus 3, Hamburg, Germany, and SustAInLivWork Center of Excellence, e-mail: michael.meyling@tuhh.de
L. Maack, Institute of Medical Technology and Intelligent Systems, Hamburg University of Technology, Hamburg, Germany
L. Miščikas, The Hospital of Lithuanian University of Health Sciences Kauno klinikos, Kaunas, Lithuania, and SustAInLivWork Center of Excellence
M. Rojas, Kaunas University of Technology, Kaunas, Lithuania, and SustAInLivWork Center of Excellence
T. Maurer, Martini-Klinik, Hamburg, Germany
S. Latus, A. Schlaefer, Institute of Medical Technology and Intelligent Systems, Hamburg University of Technology, Hamburg, Germany, and SustAInLivWork Center of Excellence

timation of the ɣ-probe's sensing area [7], and most recently, localization of a radionuclide target using adaptive scanning guided by a reinforcement learning approach [4].
Although these methods have demonstrated promising initial results, they have relied on simplified assumptions regarding target location and background activity. In clinical reality, however, radionuclides frequently accumulate in surrounding organs, significantly complicating accurate localization of the target source [8].

Addressing the challenge of locating a target in the presence of severe background activity, this work employed a convolutional neural network (CNN), which have shown exceptional performance in the similar context of radioactive dose modeling [9]. It was systematically investigated how the localization of a target is influenced by background activity, by the location of the target, and by radionuclides accumulating in the bladder. Furthermore the impact of available ɣ-probe poses was assessed. For the training and evaluation, a forward model (FM) simulated measurement data based on measurements with a real ɣ-probe and a real test source.

2 Methods

2.1 Data Generation

FM: The FM simulated the measured signal for known ɣ-probe poses and radionuclide source positions. It considered source locations, source activity, stochastic nature of decay, attenuation, ɣ-probe location, ɣ-probe orientation, and ɣ-probe geometry [10], [4]. The detected intensity I was modeled as:

$$I = C \cdot \xi \cdot A \cdot \frac{S}{d^2} \cdot e^{-\mu\rho d} \cdot f(\theta)$$

with C being a calibrated constant, ξ a normal distribution to model the stochasticity of decay, and A the activity of the source, S the active sensing area of the sensor. μ and ρ were attenuation and density coefficients, d the distance between source and ɣ-probe, θ as the angle between the ɣ-probe's viewing direction and the radiation direction. The angular sensitivity function of the ɣ-probe based on its full width half maximum (FWHM) and θ was

$$f(\theta) = e^{\left(-4\ln 2\left(\frac{\theta}{\mathrm{FWHM}}\right)^2\right)}.$$

The constants were estimated with a drop-in ɣ-probe (Lightpoint Medical Ltd.) and real measurements from different distances and angles to a radioactive test source with 1 MBq.

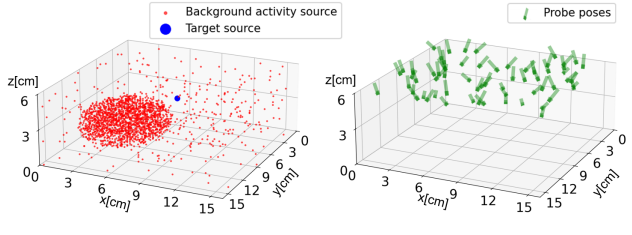

Fig. 2: Left: Example source distribution with the bladder. **Right:** Example ɣ-probe poses, at which the FM evaluates activity.

Volume definition: A 64x64x24 voxel volume with 0.25 cm^3 voxel size, corresponding to typical target sizes and investigated volumes, represented the abdominal tissue volume. Within it, the radionuclide sources were distributed.

Source distributions: To study the influence of background activity, target source location, and radionuclides accumulated in the bladder, two scenarios were modeled: Scenario 1) Based on our radioactive test source, a single 1 MBq point source representing the target was randomly positioned in the volume. Then, M point sources with an assumed activity of 10 kBq each were randomly distributed within the volume to simulate non-specific background activity.
Scenario 2) In the second scenario, the background sources were arranged to approximate a bladder-shaped volume using an ellipsoidal distribution. This bladder model varied in volume, shape, number of sources, and spatial location. An additional 400 point sources were randomly distributed throughout the tissue volume, resulting in a total of M sources at 10 kBq each. As in the first case, a 1 MBq target source was randomly placed in the volume, explicitly outside the modeled bladder region.

ɣ-probe poses: The ɣ-probe poses used for activity evaluation were semi-randomly sampled. All ɣ-probe positions were located above the tissue volume in the anterior direction, simulating measurements taken from the pneumoperitoneum. While orientations varied randomly, all poses pointed downward into the tissue toward its center.

Training, validation, and test sets: Two separate training sets were generated: one for scenario 1) involved a target source embedded in non-specific background activity, and one for scenario 2) where the target source was near the bladder. Each training set contained 142 000 distinct source distributions with varying numbers of background activity sources M. For every distribution, the forward model was evaluated at varying numbers N of randomly sampled ɣ-probe poses, that determined how many measurements are used for a single prediction. Seven different values of N were considered per distribution, resulting in approximately 1 000 000 training samples that included both the measurements and the corresponding target positions.

Independent validation sets, each containing 100 000 samples, were created for both scenarios to fine-tune the network.
For evaluation, multiple test sets were constructed. For the first scenario, 42 test sets were generated by varying the number of background sources M and the number of available ɣ-probe poses N, spanning six values of M and seven values of N. For the bladder scenario, a separate test set with a fixed bladder configuration and random target placements was created. Each of the 43 test sets contained 20 000 samples with 20 000 random target locations.

2.2 CNN

The CNN, illustrated in Figure 1, was designed to predict the 3D coordinates of a target source based on ɣ-probe measurements represented as 2D images.
Input: The input to the network was a five-channel 2D image. The spatial position of each ɣ-probe measurement in the x-y plane was encoded in the image coordinates. The first channel contained the measured signal, the second encoded the z-coordinate of the ɣ-probe pose, and the remaining three channels represented the orientation of the ɣ-probe during measurement.
Output: The network output was the predicted location (x, y, z) of the target point source.
Architecture: The CNN comprised four blocks, each containing a 2D convolutional layer with 3×3 kernels (padding 1), followed by a rectified linear unit (ReLU) activation and a max pooling layer with stride 2. The number of kernels in the convolutional layers increased progressively (32, 64, 128, and 256). The output of the final convolutional block was flattened and passed through four linear layers with 512, 128, 64, and 3 neurons, respectively, each followed by ReLU activations except the last. The final output layer produced the predicted coordinates.
Loss: The network was trained using the root mean squared error (RMSE) between the predicted and true source position:

$$\mathrm{RMSE} = \sqrt{\frac{1}{3} \cdot ((x - \hat{x})^2 + (y - \hat{y})^2 + (z - \hat{z})^2)}$$

Optimizer: The model was optimized using the Adam optimizer with a learning rate of 0.003.

2.3 Evaluation

The localization was evaluated using the Euclidean distance (ED) between the predicted and true positions of the target source as a measure of localization error:

$$\mathrm{ED} = \sqrt{3} \cdot \mathrm{RMSE}$$

The localization error was analyzed with respect to the number of background sources M, the spatial location of the target within the tissue volume (both scenario 1), and the influence of a bladder (scenario 2). The latter was examined with a focus on the distance between the target source and the bladder structure. Additionally, the influence of available ɣ-probe poses N was assessed.

3 Results

Figure 3 illustrates the influences of available ɣ-probe poses, background activity, and target location on the localization task. More ɣ-probe poses N reduced the localization error down to 0.61 cm with N = 1024 and M = 108. The improvement decreased for higher N and tended to plateau after N = 484. An increase in the number of background sources M lead to a corresponding rise in localization error. Specifically, increasing the background activity from a low-activity scenario ($M = 108$, total activity 1.08 MBq) to a high-activity scenario ($M = 3872$, total activity 38.72 MBq) resulted in an average increase in Euclidean distance (ED) of 2.86 cm. Even under optimal conditions with $N = 1024$ ɣ-probe poses, the error increased by 2.28 cm (374%) under high background activity. Additionally, the figure reveals that targets located deeper than 3 cm within the tissue were associated with a significantly higher ED. The average error increased by up to 1.82 cm (281%) from superficial to deep targets.

Figure 4 highlights the impact on localization when introducing a bladder with accumulated radionuclides. Again, more ɣ-probe poses improved localization. Regarding background activity, an accumulation with 1536 background point sources in the bladder (total activity 15.36 MBq) led to an average increase in ED of 0.73 cm compared to scenario 1) without the bladder. For the setting with the highest number of ɣ-probe

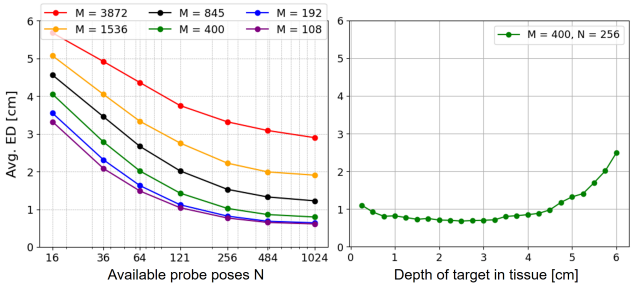

Fig. 3: Localization performance for a target source embedded in non-specific background activity. **Left:** Average Euclidean distance (ED) between predicted and true source position for varying numbers of background sources M and ɣ-probe poses N. **Right:** Average ED as a function of target depth within the tissue volume.

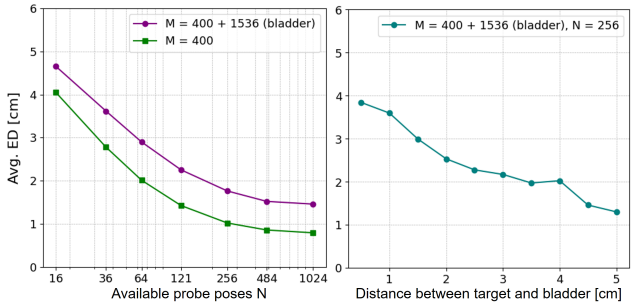

Fig. 4: Effect of a bladder on localization accuracy. **Left:** Average Euclidean distance (ED) for scenarios with a bladder (purple) compared to scenarios without it (green). **Right:** Average ED as a function of distance between the target source and the bladder.

poses ($N = 1024$), this corresponded to an increase of 81%. Furthermore, the spatial relationship between the bladder and the target played a critical role: if the target was located more than 4.5 cm away from the bladder, the average ED remained below 1.5 cm. In contrast, when the target was within 1 cm of the bladder, the ED increased to 3.72 cm, reflecting a 221% increase.

4 Discussion and Conclusion

This study investigated whether a target with high background activity in the context of radioguided surgery can be localized with a CNN. Specifically, the influence of ɣ-probe pose availability, background activity level, source location, and the presence of bladder-accumulated radionuclides was assessed.

The results demonstrated that a CNN utilizing multiple ɣ-probe measurements can predict the target source despite significant background interference. Increased background activity notably impaired localization performance, and the spatial relationship between the target and tissue surface—especially its distance from the bladder—was a key factor affecting localization error.

It is important to note that the number of ɣ-probe positions evaluated here is limited in clinical scenarios. In addition, a simplified model was used for radionuclide distribution in the bladder, and no other organs were included in the simulation. Therefore, future research on target localization in radioguided surgery should consider a limited number of ɣ-probe poses and more realistic background activity distributions. If similar performance can be achieved under these conditions, the experiment could be translated into a fully practical setup with a real ɣ-probe and radiation sources. The proposed CNN-based approach offers a promising solution for robust localization in such environments.

Author Statement

This work was partially co-funded by the European Union under Horizon Europe programme grant agreement No. 101059903; and by the European Union funds for the period 2021-2027.

The authors thank Telix Pharmaceuticals Ltd. for providing the ɣ-probe and the test source.

References

[1] Cornford, P., van den Bergh, R.C., Briers, E., Van den Broeck, T., Brunckhorst, O., Darraugh, J., et al. Eau-eanm-estro-esur-isup-siog guidelines on prostate cancer—2024 update. part i: Screening, diagnosis, and local treatment with curative intent. European Urology 2024;86(2):148–163.

[2] van Oosterom, M.N., Simon, H., Mengus, L., Welling, M.M., van der Poel, H.G., van den Berg, N.S., et al. Revolutionizing (robot-assisted) laparoscopic gamma tracing using a drop-in gamma probe technology. American Journal of Nuclear Medicine and Molecular Imaging 2016;6(1):1–17.

[3] Berrens, A.C., Knipper, S., Marra, G., van Leeuwen, P.J., van der Mierden, S., Donswijk, M.L., et al. State of the art in prostate-specific membrane antigen-targeted surgery—a systematic review. European Urology Open Science 2023;54:43–55.

[4] Zhang, H., Deng, K., Hu, Z.J., Huang, B., Elson, D.S.. Hybrid deep reinforcement learning for radio tracer localisation in robotic-assisted radioguided surgery. arXiv (accepted to IEEE International Conference on Robotics & Automation) 2025;.

[5] Falkenbach, F., Mazzucato, G., Schmalhofer, M.L., Tian, Z., Karakiewicz, P.I., Graefen, M., et al. Robot-assisted psma-radioguided surgery for local recurrence in the prostatic bed. BJU International 2025;Epub ahead of print.

[6] Fuerst, B., Sprung, J., Pinto, F., Frisch, B., Wendler, T., Simon, H., et al. First robotic spect for minimally invasive sentinel lymph node mapping. IEEE Transactions on Medical Imaging 2016;35(3):830–838.

[7] Huang, B., Hu, Y., Nguyen, A., Giannarou, S., Elson, D.S.. Detecting the sensing area of a laparoscopic probe in minimally invasive cancer surgery. In: International Conference on Medical Image Computing and Computer-Assisted Intervention. Springer; 2023, p. 260–270.

[8] Dell'Oglio, P., De Barros, H., Maurer, T., Wit, E., Stricker, P., van der Poel, H., et al. Robotic radioguided surgery using a drop-in gamma probe-technical insights for different prostate cancer indications. 2021.

[9] Lee, M.S., Hwang, D., Kim, J.H., Lee, J.S.. Deep-dose: a voxel dose estimation method using deep convolutional neural network for personalized internal dosimetry. Scientific Reports 2019;9(1):10308.

[10] Hartl, A., Shakir, D.I., Lasser, T., Ziegler, S.I., Navab, N.. Detection models for freehand spect reconstruction. Physics in Medicine and Biology 2015;60(3):1031–1046. Epub 2015 Jan 14.